Available online at www.sciencedirect.com
SCIENCE DIRECT
Precision Engineering 28 (2004) 338–357
PRECISION ENGINEERING
www.elsevier.com/locate/precision

Design of quasi-kinematic couplings

Martin L. Culpepper*
MIT Department of Mechanical Engineering, 77 Massachusetts Avenue, Room 3-449b, Cambridge, MA 02139, USA

Received 27 May 2002; accepted 16 December 2002

Abstract

A quasi-kinematic coupling (QKC) is a fixturing device that can be used to make low-cost assemblies with sub-micron precision and/or sealing contact. Unlike kinematic couplings that form small-area contacts between mating balls in v-grooves, QKCs are based on arc contacts formed by mating three balls with three axisymmetric grooves. Though a QKC is technically not an exact constraint coupling, proper design of the contacts can produce a weakly over constrained coupling that emulates an exact constraint coupling. This paper covers the practical design of QKCs and derives the theory that predicts QKC stiffness. A metric used to minimize over constraint in QKCs is presented. Experimental results are provided to show that QKCs can provide repeatability (1/4 μm) that is comparable to that of kinematic couplings.

Keywords: Kinematic coupling; Quasi-kinematic coupling; Plastic deformation; Exact constraint; Fixture; Repeatability; Stiffness; Assembly; Photonics; Automotive assembly; Over constraint; Precision optics

1. Introduction

1.1. Background

The need to improve performance has forced designers to tighten alignment tolerances for next generation assemblies. Where tens of microns were once sufficient, nanometer/micron-level alignment tolerances are becoming common. Examples can be found in automotive engines, precision optics and photonic assemblies. Unfortunately, the new alignment requirements are beyond the practical capability (~5 μm) of most low-cost alignment technologies. The absence of a low-cost, sub-micron coupling has motivated the development of a new class of coupling interface, the quasi-kinematic coupling (QKC) (Fig. 1A).

1.2. The need for a new precision coupling

To understand the need for a new class of precision fixtures, it is necessary to understand why the cost and performance characteristics of current technologies are incompatible with the dual requirements of low-cost and sub-micron precision. We will first examine coupling types used in traditional manufacturing. The most common type, the pinned joint, is formed by mating pins from a first component into corresponding holes or slots in a second component. Obtaining micron-level precision with these couplings is impractical due to the micron-level tolerances that are required on pins, holes and pin–hole patterns. Other well-known couplings such as tapers, dove–tails and rail–slots would also require micron-level tolerances. They also require expensive finishing operations to reduce the effect of surface finish on alignment performance.

Let us now consider exact constraint couplings that are well known in precision engineering, but less frequently used in manufacturing. A common type of exact constraint coupling, a kinematic coupling (see Fig. 1A), routinely provides better than 1 μm precision [1] alignment. Unfortunately, they fail to satisfy three low-cost coupling requirements that are common to many manufacturing processes:

1. *Low-cost generation of fine surface finish*: micron-level kinematic couplings must use balls and grooves with ground or polished surfaces [2]. Although balls with fine surface finish are generally inexpensive, grooves with fine surface finish are expensive. The finishing operations used to prepare groove surfaces add considerable cost to kinematic couplings.
2. *Low-cost generation of alignment feature shape*: making v-grooves for kinematic couplings requires more time and more complicated manufacturing processes than required by present low-cost technologies, i.e. pinned joints. For example, the ball and grooves are geometrically more complex, with more tolerances than pins and holes. Likewise, high-hardness balls and grooves are

* Tel.: +1-617-452-2395; fax: +1-509-693-0833.
E-mail address: culpepper@mit.edu (M.L. Culpepper).

0141-6359/$ – see front matter © 2004 Elsevier Inc. All rights reserved.
doi:10.1016/j.precisioneng.2002.12.001

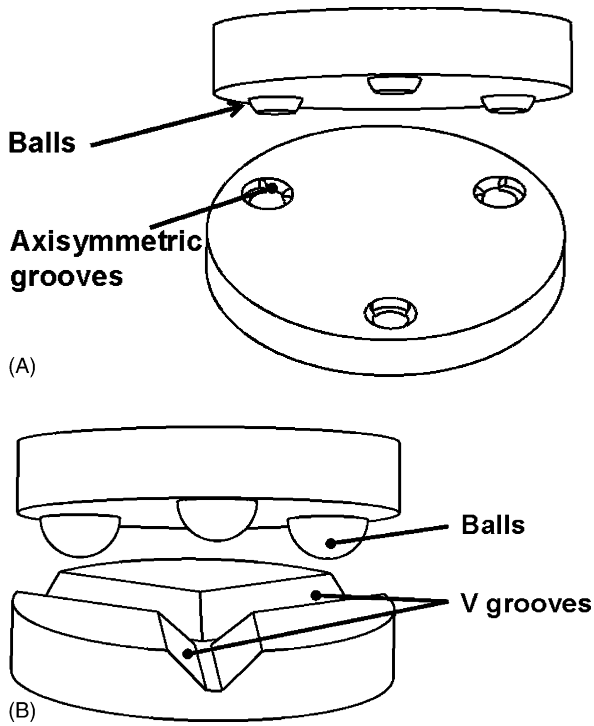

Fig. 1. Quasi-kinematic (A) and kinematic (B) couplings.

desired to withstand Hertzian contact stresses at the contact regions [2]. These materials require additional effort to harden and/or machine.

3. *Low-cost means to form sealed interfaces*: kinematic couplings are not generally meant to form sealed interfaces unless they are equipped with flexures [3,4] that add cost and complexity.

Having covered common manufacturing couplings and kinematic couplings, we now compare their cost and performance. Fig. 2 shows a clear performance gap between low-performance/low-cost couplings and high-performance/moderate-cost couplings. Clearly, the gap must be addressed if alignment is to be removed as the main obstacle to enabling low-cost, high-precision assemblies. The QKC was designed to address this gap.

1.3. Contents

Section 2 discusses the concept of the QKC and shows how it satisfies the low-cost coupling requirements in Section 1.2. Section 3 provides the theory used to predict coupling stiffness and provides a metric that can be used to minimize over

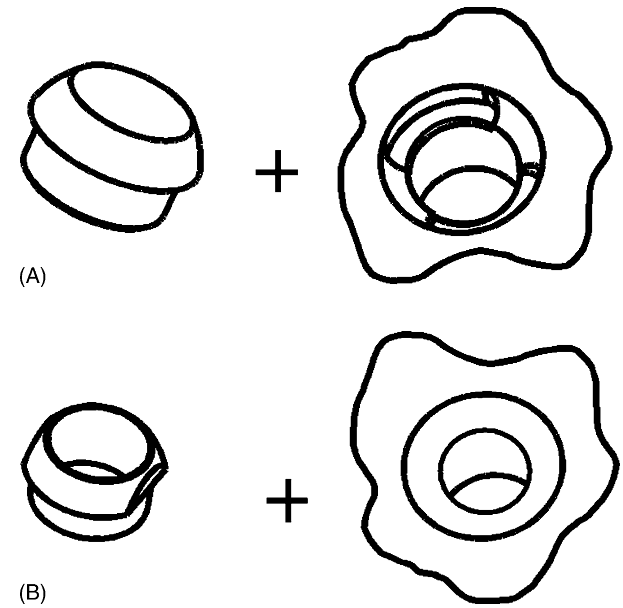

Fig. 3. Relieved groove (A) and relieved ball (B) QKC joint designs.

constraint in QKCs. Section 4 discusses the theory as implemented in a MathCAD program and Section 5 provides experimental results that show QKCs can provide performance comparable to exact constraint couplings. The implications of coupling cost are covered in Section 6. Appendices are provided to cover the details of the theory and the design tool.

2. Quasi-kinematic coupling concept

2.1. Similarities and differences between kinematic and quasi-kinematic couplings

From Fig. 1, we see that kinematic and QKCs share similar geometric characteristics. A kinematic coupling consists of balls attached to a first component that mate with v-grooves in a second component. The balls and grooves form small-area contacts. QKCs consist of axisymmetric balls attached to a first component that mate with axisymmetric grooves in a second component. Here the balls and grooves form arc contacts. Two examples of axisymmetric geometries that form arc contacts are shown in Fig. 3. The orientation of joints in both couplings is also similar. To achieve good stability and balanced stiffness, joints are oriented with ball–groove contacts in symmetric positions and orientations with respect to the bisectors of the coupling triangle [2].

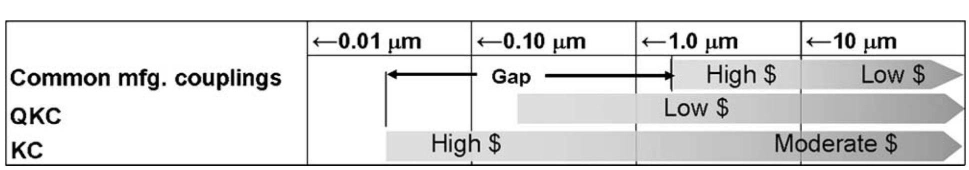

Fig. 2. Cost and precision of common couplings.

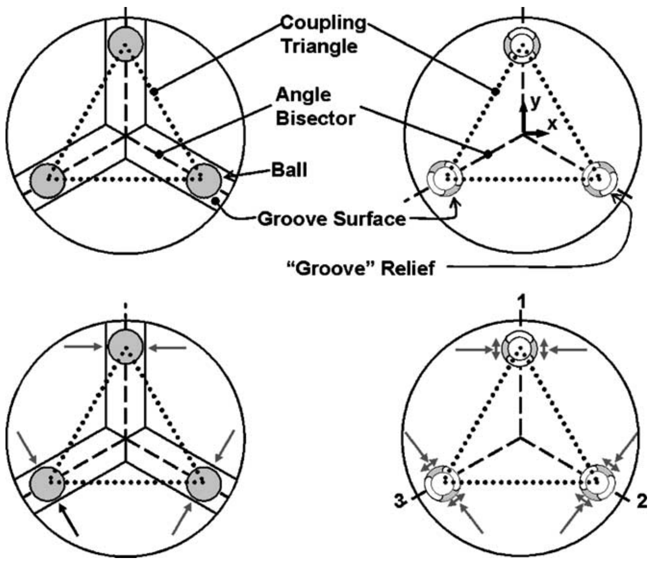

Fig. 4. Planar constraints in kinematic (left) and quasi-kinematic (right) couplings.

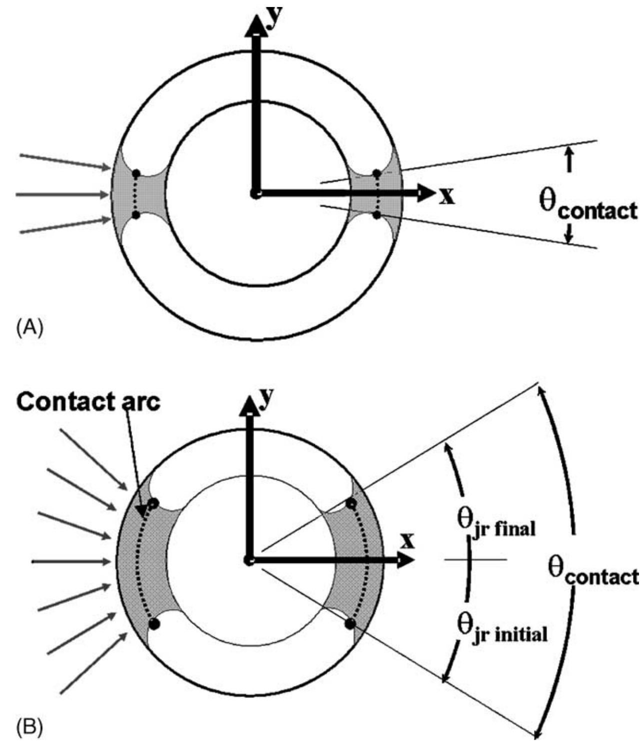

Fig. 5. The link between $\theta_{contact}$ and over constraint in QKCs with (A) small $\theta_{contact}$ and (B) large $\theta_{contact}$.

The fundamental difference between kinematic couplings and QKCs lies in the nature of the ball–groove contacts. Ideal kinematic couplings establish six localized contacts that provide well-defined constraint in desired directions and permit the freedom of motion in other directions. QKCs use ball and groove geometries which are symmetric and thus easier to manufacture, but depart from the constraint characteristics of ideal kinematic couplings by using arc contacts rather then small-area contacts. With careful design, QKCs can be made to emulate the performance of kinematic couplings.

With this goal in mind, we must understand how QKC constraints differ from ideal kinematic coupling constraints (Fig. 4). In this figure, we see the projections of ball–groove contact forces on the plane of coupling. The length of an arrow signifies the magnitude of a given constraint force. Fig. 4 (left) shows an ideal kinematic coupling which provides constraint between the balls and grooves in directions normal to the bisectors of the coupling triangle. Freedom of motion is permitted parallel to the bisectors. This is sufficient to achieve stable, exact constraint coupling [2]. Fig. 4 (right) indicates that the arc contacts of the QKC provide desired constraint perpendicular to the bisector and some constraint along the bisectors. Without freedom of motion parallel to the bisector, the coupling will have some degree of over constraint.

The key to designing good QKCs is to minimize over constraint by minimizing the contact angle, $\theta_{contact}$. The contact angle is defined by illustration in Fig. 5. The half angle, θ_{jr} will be used in the theoretical derivation in Appendix A. The joint in Fig. 5 represents joint 1 in Fig. 4. Arrows representing the constraint per unit length of contact arc are shown on the left sides of Fig. 5A and B. By inspection, we can see that constraint contributions that are parallel to the angle bisectors (in the y direction) can be reduced by making the contact angle smaller. This in turn reduces the degree of over constraint the joint may impose on the coupling. Unfortunately, this reduces coupling stiffness. This stiffness-constraint trade-off requires a quantitative metric to optimize coupling design. We will improve our qualitative understanding with a quantitative metric in Section 3.2. For now we continue with a qualitative assessment of QKC attributes.

2.2. QKCs that satisfy low-cost coupling requirements

We now assess the performance of QKCs with respect to the low-cost coupling requirements given in Section 1.2.

1. *Low-cost generation of fine surface finish*: QKC balls can be made from low-cost, polished spheres (i.e. bearings). By applying sufficient mating force, one can burnish the surface of the groove by pressing the harder, finer surface of the ball into the groove surface. The result of this burnishing process is shown in Fig. 6. A successful burnishing operation has two important requirements:
   - A ball with polished (or ground if sufficient) surface finish and Young's modulus three to four times that of the groove [5].
   - Tangential sliding between the ball and groove surfaces [6] during mating. Contact without tangential sliding does not entirely remove asperities [7].
2. *Low-cost generation of alignment feature shape*: QKC grooves are axisymmetric, thus they can be made in a "plunge/drill" operation using a counter sink or form tool.

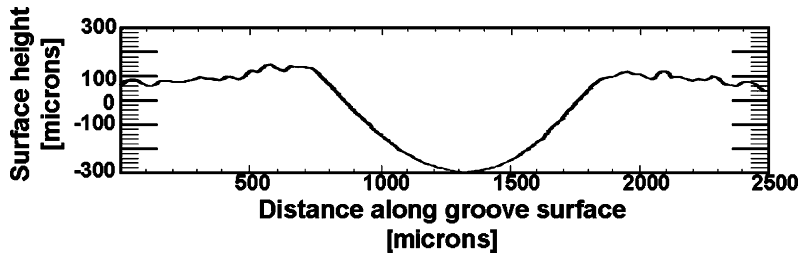

Fig. 6. Surface trace of burnished QKC groove.

Groove reliefs can be cast, formed, milled, or drilled in place. The tools and processes required to form the groove seats are comparable to those required to make pinned joints.

3. *Low-cost means to form sealed interfaces*: it is possible to enable sealing contact by integrating compliance into a QKC joint. Using the joint design in Fig. 7A and B, we add *z* compliance via the hollow core and side undercut.

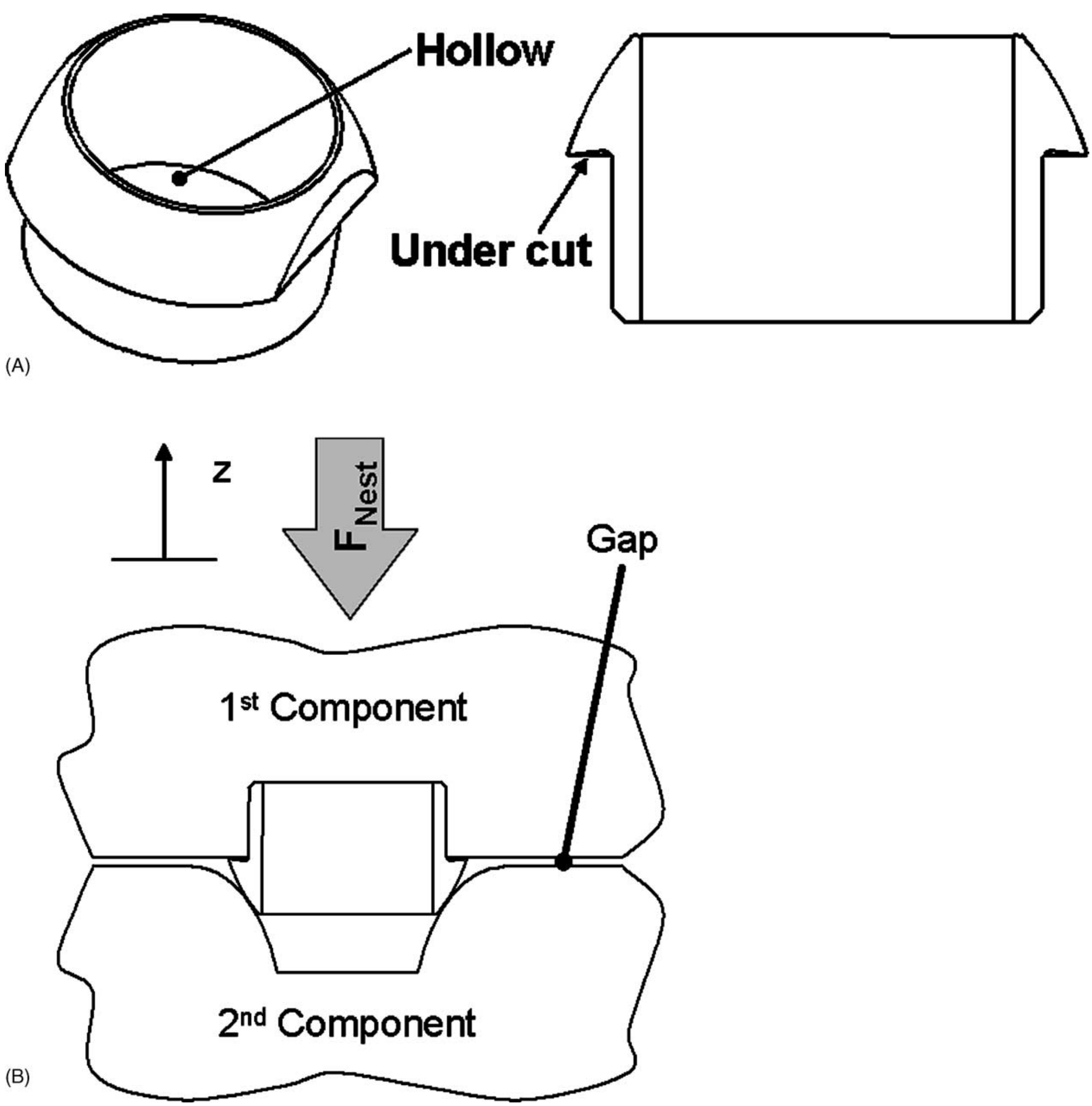

Fig. 7. Geometry of (A) compliant quasi-kinematic ball and (B) cross-section of a QKC joint.

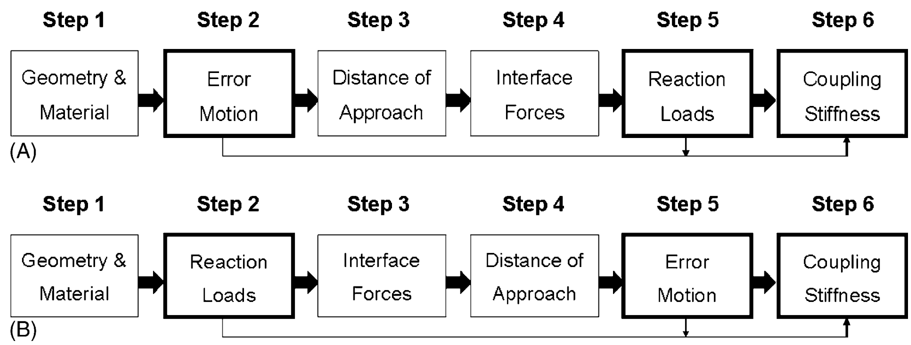

Fig. 8. Stiffness modeling strategies for (A) quasi-kinematic and (B) kinematic couplings.

As shown in Fig. 7B, a nesting force mates the balls and grooves. By increasing the nesting force, we can deform the ball–groove joints until the gap separating the coupled components closes. Gaps of several hundred microns can be closed if the ball–groove materials plastically deform during the first mate. When the coupling is unloaded, elastic recovery of the ball and groove materials restores a portion of the gap between the mated components. Retaining a portion of the gap between components is necessary to maintain the kinematic nature of the coupling in subsequent mates.

3. Theory of quasi-kinematic couplings

3.1. Analysis method

When analyzing kinematic couplings, contact forces and displacements may be assumed normal to the ball–groove contact and modeled with “spring like” Hertzian point contacts [2,8–10]. When analyzing arc contacts, the direction of contact forces may not be assumed and the contacts cannot be modeled as point contacts. An appropriate analysis method is outlined in Fig. 8A. We preload a coupling with a desired displacement preload, impose an error displacement on this “perfectly” mated state, calculate ball–groove contact forces and then use these forces and the error displacements to calculate coupling stiffness.

This is a significant departure from the method (Fig. 8B) used to evaluate ideal kinematic coupling stiffness. A detailed derivation of the kinematic and mechanics theories used to model the performance and characteristics of QKCs is provided in Appendix A. This theory is used to develop the metrics and charts which appear in the following sub-sections and the design tool provided in Appendix B.

3.2. Constraint metric

In Section 2.1 we learned that the geometry of the arc contacts leads to some degree of over constraint in QKCs. There are a variety of other factors (for instance friction, geometry, etc.) that may add to the degree of over constraint in a precision coupling. Our interest here is in developing a means to understand how the ball–groove arc contacts can be designed to optimize the performance characteristics of a quasi-kinematic joint. We will use the constraint metric as defined in Eq. (1).

Table 1
Example QKC joint design characteristics

Design variable	Value
R_c	0.66 cm (0.260 in.)
δ_z-preload	$-60\ \mu$m (-0.002 in.)
K	$1 \times 10^{-2}(\text{N}/\mu\text{m}^{2.07})$ $(2948850(\text{lb/in.}^{2.07}))$
b	1.07
θ_{contact}	120°
θ_c	45°

$$\text{CM}_i = \frac{\text{Stiffness parallel to bisector}}{\text{Stiffness perpendicular to bisector}} = \frac{k_{i\ ||\text{Bisector}}}{k_{i\ \perp\text{Bisector}}} \quad (1)$$

Let us consider the relieved groove joint design described by Fig. 9A and Table 1. The joint’s radial stiffness plot, shown in Fig. 9B, was generated using the theory in Appendix A. We can use numerical results from the theory, where $\theta_{\text{contact}} = 120°$ (or estimate values from Fig. 9B) to determine the constraint metric for this joint.

$$\text{CM} = \left.\frac{k(90°)}{k(0°)}\right|_{\text{Fig. 9}} = \frac{80\ \text{N}/\mu\text{m}}{195\ \text{N}/\mu\text{m}} = 0.41 \quad (2)$$

This ratio is useful as a metric for reducing the potential for over constraint based on the joint’s mechanics (stiffness and material) characteristics. A full estimate of the alignment error due to over constraint ($\delta_{\text{over constraint}}$) would need to consider kinematic characteristics, e.g. the post-plastically deformed mismatch between the ball and groove patterns ($\delta_{\text{final-mismatch}}$). Current efforts are focused on developing a means to relate the error and mismatch by means of the following equation.[1]

$$\delta_{\text{over constraint}} = f(\delta_{\text{final-mismatch}} \times \text{CM}) \quad (3)$$

Unfortunately, the mismatch between QKC joints depends on (1) elastic contact deformation, (2) plastic deformation and (3) multiple ball–groove mismatch tolerances. The theory

[1] The author thanks Dr. Layton Hale for bringing this form of this equation to his attention.

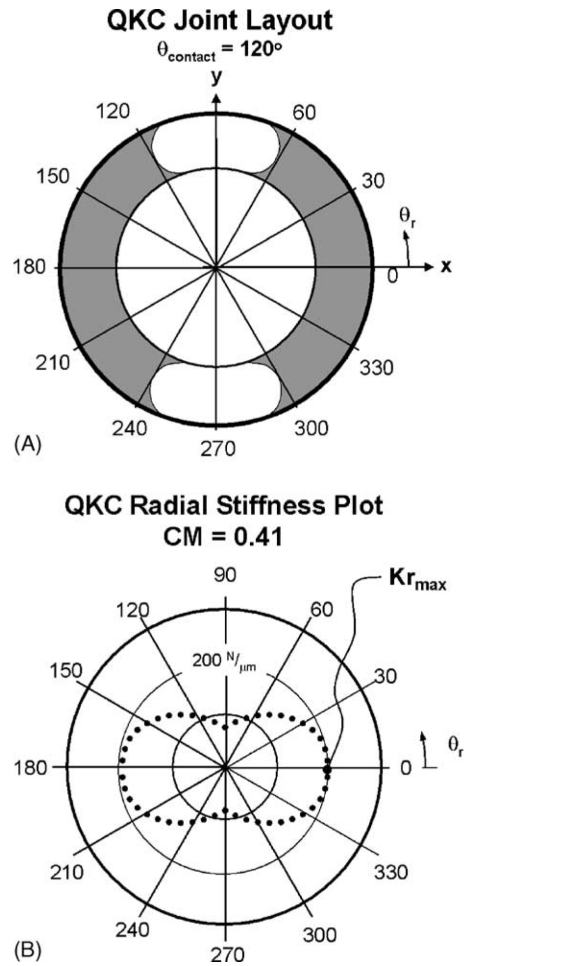

Fig. 9. Example QKC relieved groove (A) orientation and (B) stiffness for $\theta_c = 45^\circ$; $\theta_{\text{contact}} = 120^\circ$; $K\,(\text{N}/\mu\text{m}^{2.07}) = 1 \times 10^{-2}$; $b = 1.07$; $R_c = 0.66$ cm; $\delta_{\text{z-preload}} = -60\,\mu$m.

capable of describing the final mismatch has yet to be developed. We will continue with the mechanics-based constraint metric as this is immediately useful as a key element in minimizing the potential for over constraint during the design process.

3.3. Making use of the constraint metric

In QKCs, the CM is unity for $\theta_{\text{contact}} = 180^\circ$ (gross over constraint) and approaches 0 as $\theta_{\text{contact}} \to 0^\circ$. The desire to emulate exact constraint couplings compels us to specify the lowest possible contact angle. It is clear however, that one can not specify $\theta_{\text{contact}} \sim 0^\circ$ and obtain a coupling with reasonable stiffness. The key is simultaneous consideration of the constraint metric and the coupling's stiffness in directions of interest. We will demonstrate this approach via a hypothetical application.

Consider a 120° coupling (grooves spaced at 120°) that must resist z moments about its' centroid. The design calls for 125 N/µm as the lowest value for the maximum radial stiffness of a joint ($K_{r_{\max}}$ would be 195 N/µm in Fig. 9B). The

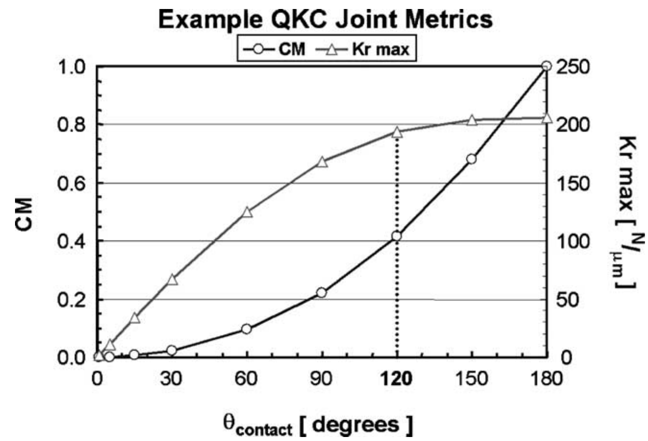

Fig. 10. Comparing performance metrics of QKCs.

plot in Fig. 10 shows the effect of θ_{contact} on our constraint metric and coupling stiffness. Given this plot, we could justify choosing a contact angle as low as 60° with a CM = 0.10. It is interesting to note that the trade-off between stiffness and constraint is a favorable transaction at large contact angles.

4. Testing the MathCAD model

The theory developed in Appendix A was implemented in the MathCAD program provided in Appendix B. The model was checked by running the following tests:

- Imposed translation errors in the z direction produced only net z forces.
- Imposed rotation errors about the z axis of the coupling centroid produced only z moments.
- Imposed displacements along one bisector of a 120° coupling (i.e. in the y direction for the coupling in Fig. 4) did not produce net y or z moments.
- The x and y reaction forces are 0 when θ_c is 90° (groove becomes a flat).
- When given inputs that would make the ball loose contact with the groove, the model detects this as a violation of a "constant contact" constraint (see Appendix B, "Verify Constant Contact Condition").

5. Experimental results

A form of QKC has been used in precision automotive assemblies to provide 2/3 µm repeatability in journal bearing assemblies [11–13]. To meet unusual stiffness requirements, the joints were not placed in the orientations that best emulate exact constraint couplings. These joints were also designed with large contact angles ($\theta_{\text{contact}} = 120^\circ$, CM = 0.41) to increase coupling stiffness. Though this design serves as proof of sub-micron performance, it is not a good means to demonstrate the best performance of QKCs.

An experiment was run to determine how repeatability of a QKC would compare to that of an ideal kinematic coupling when the QKCs contact angle and joint orientations were set to better emulate an ideal kinematic coupling. Table 1 lists the characteristics for the joints used in the experiment. For the test, the contact angle, $\theta_{contact}$, was set to 60° and thus the constraint metric as read from Fig. 10 is 0.10. This joint design retains the low-cost attributes of the quasi-kinematic joint used in [11–13] and is closer in constraint characteristics to ideal kinematic couplings and kinematic couplings with flexures [10,14].

The test coupling in Fig. 11A was manufactured with less than 25 μm mismatch between the axis of symmetry of any ball and mated groove. The results of repeatability tests with lubricated joints are provided in Fig. 11B. The results show the coupling repeats in-plane to 1/4 μm after an initial wear-in period. When this wear-in period is not practical, one may use a preload which induces plastic deformation of the ball–groove surfaces. This has been shown to eliminate this wear in period and eliminate the mismatch between ball and groove patterns [12]. These results compare more favorably with the sub-micron performance (0.10 μm) of well designed and lubricated kinematic couplings [15].

6. Coupling cost

The QKC elements used in the automotive assemblies and test coupling resemble the elements shown in Fig. 3A. These ball–groove sets cost approximately $1 when manufactured

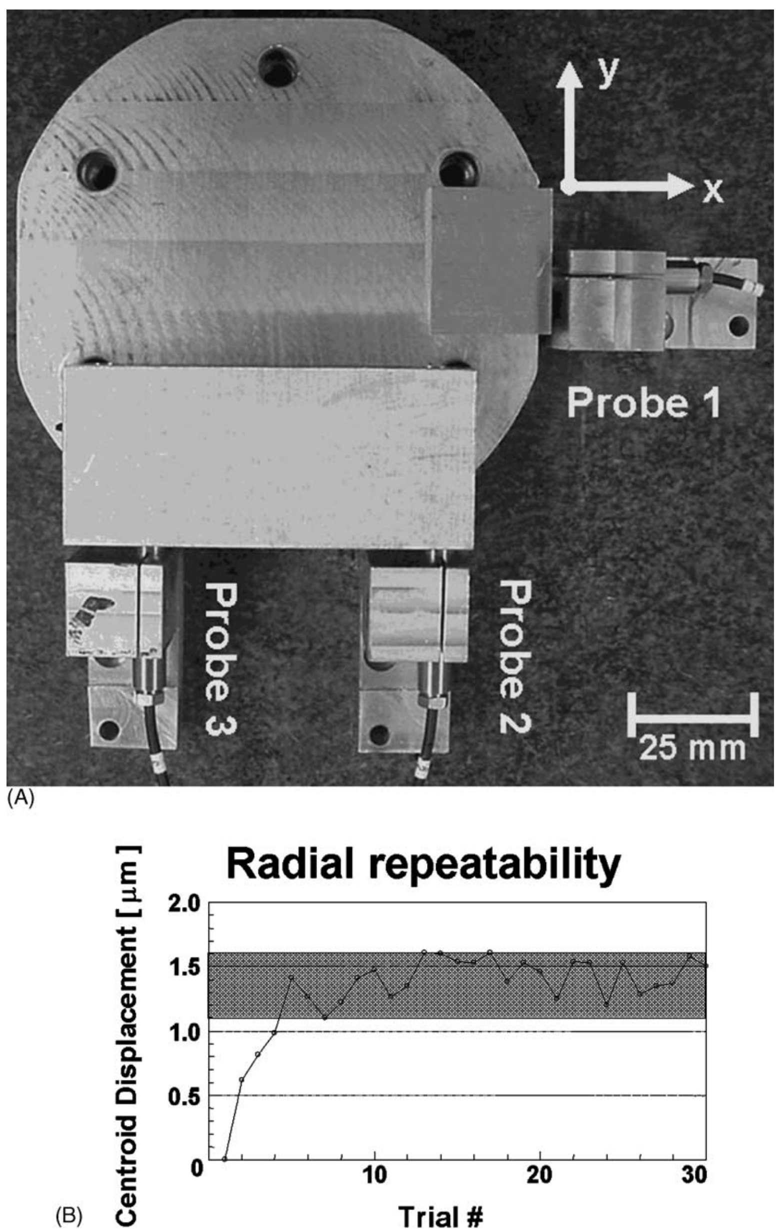

Fig. 11. QKC (A) test setup and (B) repeatability results for $\theta_c = 32°$; $\theta_{contact} = 60°$; K (N/μm$^{2.07}$) $= 1 \times 10^{-2}$; $b = 1.07$; $R_c = 0.66$ cm; 25 N preload.

in volumes greater than 100,000 couplings per year. When manufactured in volumes of less than several hundred per year, a ball–groove set may cost $60. This is in contrast to several hundred dollars one could pay for high-performance kinematic couplings. In addition to the initial cost savings, the reduced replacement cost for the balls and grooves can provide long-term cost savings.

7. Conclusions and issues for further research

This paper has provided the theory and a mechanics-based metric that can be used by designers to minimize the degree of over constraint in QKCs. The theory used to model coupling stiffness has been implemented in MathCAD and tested. Experimental results show that properly designed QKCs can provide precision alignment that is comparable to kinematic couplings. Characteristics such as low-cost, ease of manufacture, ability to form sealed joints and sub-micron performance will make the coupling an enabling technology. This will be particularly important for high-precision, high-volume assemblies in automotive, photonics, optical and other general product assemblies. Subsequent research activities will include developing the means to estimate alignment errors due to the kinematic effects that result from mismatch between ball and groove patterns.

Acknowledgments

This work was sponsored by the Ford Motor Company. The author wishes to thank them for their financial and technical assistance.

Appendix A. Theory of quasi-kinematic couplings

The purpose of this appendix is to provide the steps in a derivation of the kinematic and mechanics theories used to model the performance characteristics of QKCs.

A.1. Step 1: material and geometry characteristics

The first step is to identify the materials which the coupling components are made of and how they will be shaped

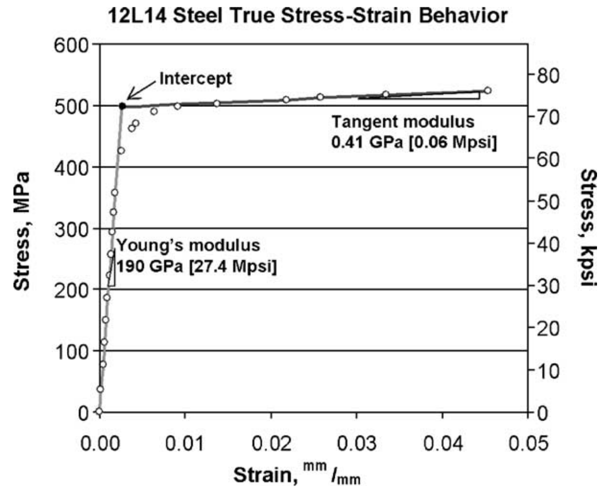

Fig. 12. Elastic–plastic behavior of 12L14 steel.

and arranged. We will assume common materials, shapes and sizes between the balls and grooves in the three joints.

A.1.1. Material characteristics

The Young's modulus and Poison's ratio of the ball and groove materials are needed to model elastic contact [16]. Modeling plastic deformation requires a tangent modulus and stress value (yield stress) up to which the Young's modulus may be used. Fig. 12 shows the values fitted to data from tests on leaded steel.

A.1.2. Geometric characteristics

With the help of Figs. 13 and 14, we define important geometry characteristics of QKCs. The first is the coupling coordinate system, CCS, which is attached to the coupling centroid of the grounded component (contains grooves). A displaced coordinate system, DCS, is attached to the centroid of the component that is displaced (contains balls) when coupling errors are present. When the coupling is mated with a preload displacement and no error motions, the CCS and DCS are coincident.

Our analysis will now utilize subscripts i and j to refer to specific joints ($i = 1$ to 3) and contact arcs ($j = 1$ to 6), respectively. We define a joint coordinate system, JCS_i, for

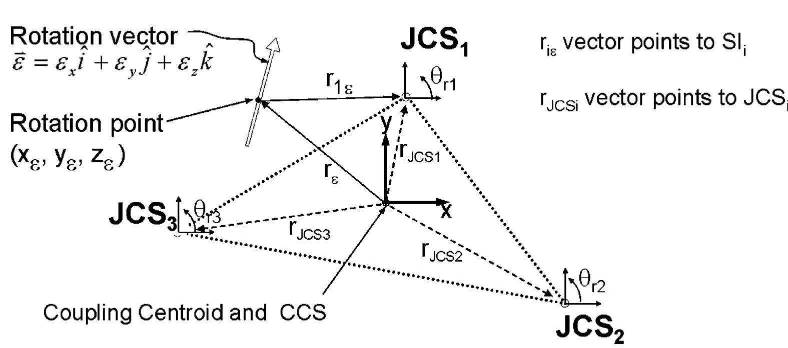

Fig. 13. Geometry characteristics of QKCs.

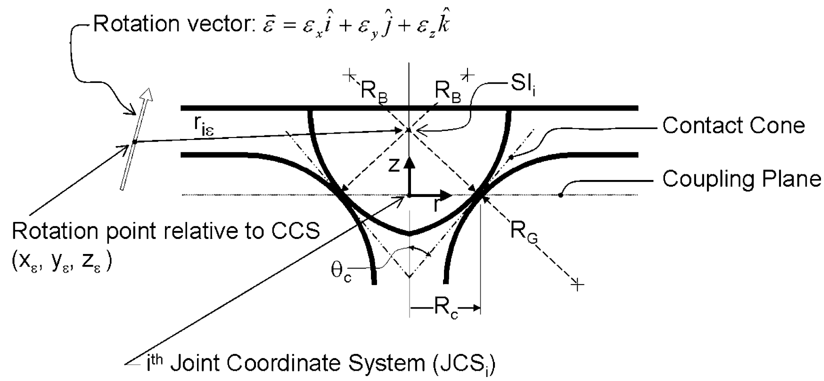

Fig. 14. Geometry characteristics of quasi-kinematic coupling joints.

each joint. Each JCS_i measures position in r_i, θ_{ri}, and z_i as collectively shown by Figs. 13 and 14. The z axis of each JCS_i is perpendicular to the coupling plane and coincident with the respective groove's axis of symmetry. For each JCS_i, $\theta_{ri} = 0$ when the projection of the joint's r vector on the x–y plane of the CCS is parallel to the x axis of the CCS. We define a contact cone as the surface which contains all lines that run through the joint's axis of symmetry and is tangent to the ball and groove surfaces at contact. The cone is characterized by the half-cone angle, θ_c. Other variables that describe the size and location of coupling components are defined by illustration in Figs. 13 and 14.

A.2. Step 2: imposed error motions

Ball–groove reaction force (therefore coupling stiffness) is a function of the compression of ball and groove material. This in turn depends on the error displacement of a ball's far field point, SI_i in Figs. 14 and 15, from its preloaded position in the groove. The displacement of a ball's SI can be expressed as a combination of the translation ($\vec{\delta}_c$) of the DCS relative to the CCS and rotation ($\vec{\varepsilon}$) of the displaced component about a specified point ($x_\varepsilon, y_\varepsilon, z_\varepsilon$). This displacement can also be given as a combination of preload displacement and error displacement of a ball's SI_i relative to the CCS. Eq. (A.1) expresses both possibilities:

$$\vec{\delta}_{SI_i} + \vec{\delta}\Big|_{\text{preload}_{SI_i}} = \vec{\delta}\Big|_{\text{error}_{SI_i}} = \vec{\delta}_c + \vec{\varepsilon} \times \vec{r}_{i\varepsilon} = \begin{bmatrix} \delta_{SI_i x} & \hat{i} \\ \delta_{SI_i y} & \hat{j} \\ \delta_{SI_i z} & \hat{k} \end{bmatrix} \tag{A.1}$$

In developing Eq. (A.1), we assume the coupling is built to limit rotation errors on the order of several microradians, thus small-angle approximations are valid. We also assume that good coupling design practices have been followed so that the coupled components can be considered as rigid bodies. The rigid body assumption requires that the mated components and their interfaces with the balls and grooves are more than 10 times as stiff as the ball–groove contacts.

A.3. Step 3: distance of approach between far field points in ball–groove joints

The compression of ball and groove material may vary about the arc contact. For example, consider a sphere mated

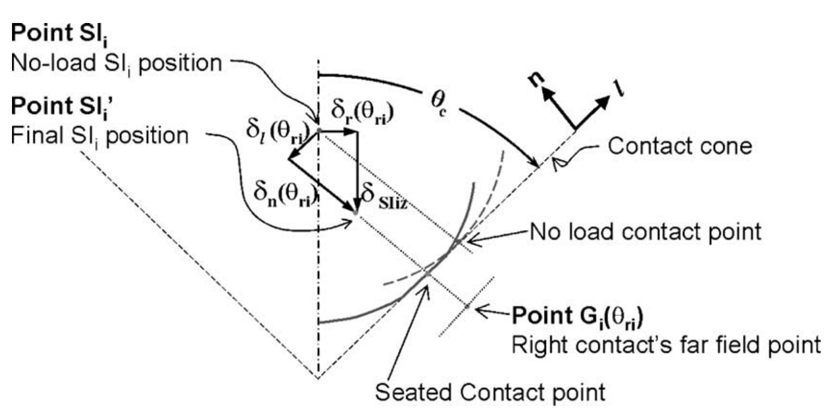

Fig. 15. Positions and motions of ball and groove far field points.

in a cone. If we displace the sphere into and along the cone's axis of symmetry the compression about the resulting circular contact will be uniform. Subsequent displacement perpendicular to the axis of symmetry will lead to variations in compression about the contact. As reaction force depends upon the compression of material, we expect the force per unit length of contact arc will vary about the ball–groove contact.

A common metric used to describe material compression between contacting elements is the distance of approach, δ_n, between two far field points [12]. Fig. 15 shows the distance of approach (as $\delta_n(\theta_{ri})$) between far field points, SI_i and $G_i(\theta_{ri})$, in a cross-section through a joint cut at θ_{ri}. The distance of approach in a cross-section is a function of the axial ($\vec{\delta}_{SI_i z}$) and radial ($\vec{\delta}_r(\theta_{ri})$) displacement of the SI_i relative to the JCS_i. Eq. (A.2) provides the axial and radial displacements as a function of ball displacement.

$$\begin{bmatrix} \delta_r(\theta_{ri}) & \hat{r} \\ \delta_{SI_i z} & \hat{k} \end{bmatrix} = \begin{bmatrix} (\delta^2_{SI_i x} + \delta^2_{SI_i y})^{0.5} \cos[\theta_{ri} - \mathrm{atan}(\delta_{SI_i y}/\delta_{SI_i x})] & \hat{r} \\ \delta_{SI_i z} & \hat{k} \end{bmatrix} \tag{A.2}$$

Using Fig. 15 and Eq. (A.2) we can produce the relationship for $\delta_n(\theta_{ri})$ given in Eq. (A.3).

$$\vec{\delta}_n(\theta_{ri}) = \left\{ -(\delta^2_{SI_i x} + \delta^2_{SI_i y})^{0.5} \cos phantom \left(\frac{\delta_{SI_i y}}{\delta_{SI_i x}} \right) \left[\theta_{ri} - \mathrm{atan}\left(\frac{\delta_{SI_i y}}{\delta_{SI_i x}} \right) \right] \cos(\theta_c) + \delta_{SI_i z} \sin(\theta_c) \right\} \hat{n} \tag{A.3}$$

A.4. Step 4: modeling interface forces as a function of δ_n

For solid ball–groove joints that experience elastic contact deformation, one may use classical line contact solutions to relate the distance of approach to the force per unit length of contact, $\vec{f}_n(\theta_{ri})$ [15,17]. A more general, flexible approach is needed to model a wide range of contact situations. For instance, consider situations with only elastic contact deformation, with contact deformation in combination with integral compliance, or with elastic and plastic contact deformation. Practical applications that use one or more of these contact situations were discussed in Section 2.2. Given the material properties and geometry characteristics from step 1, we can obtain the relationship between $\vec{f}_n(\theta_{ri})$ and $\vec{\delta}_n(\theta_{ri})$. This can be accomplished using classical line contact solutions, FEA, or other suitable analyses from which results can be fit to the form of Eq. (A.4).

$$\vec{f}_n(\theta_{ri}) = K[\delta_n(\theta_{ri})]^b \hat{n} \tag{A.4}$$

In Eq. (A.4), K is a stiffness constant and the exponent b is used to reflect the rate of change in contact stiffness with changing $\vec{\delta}_n(\theta_{ri})$. Both K and b are functions of ball–groove

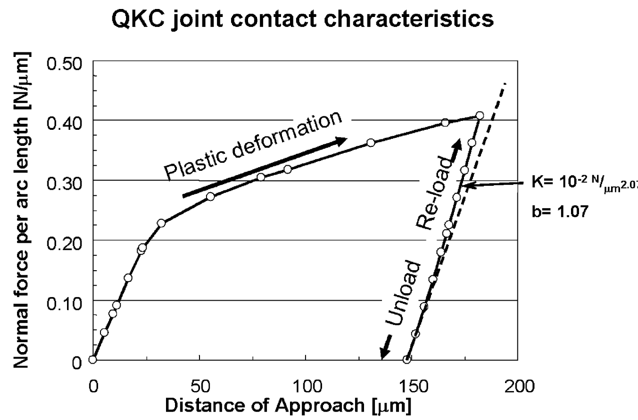

Fig. 16. Contact load–displacement (f_n vs. δ_n) behavior of a QKC joint ($\theta_c = 32^\circ$; K (N/μm$^{2.07}$) $= 1 \times 10^{-2}$; $b = 1.07$; $R_c = 0.66$ cm).

material and geometry. Let us consider an example which illustrates what Eq. (A.4) can tell us about a coupling's performance. In Fig. 16, we see the contact behavior of a joint that has experienced plastic deformation during the first mate, i.e. as needed to close a gap. In subsequent couple–uncouple cycles, the load–unload behavior of the contact follows the right most curve as indicated. The instantaneous slope of this particular curve increases with increasing preload. The geometry of the ball can be "tuned" to achieve different values of K and b, thus controlling the magnitude (K) of coupling stiffness and the non-linearity (b) of the coupling's force–displacement behavior.

To ensure that contact is not lost between the ball and groove, we monitor a "constant contact" constraint, $\vec{\delta}_n(\theta_{ri}) \leq 0$, along the arc of contact. If this is violated, the ball and groove have separated over some portion of the contact and our analysis may predict tensile contact forces. Clearly this invalidates the model.

A.5. Step 5: reaction force on an arc contact

We define a unit vector, $\hat{s}(\theta_{ri}) = \hat{n}(\theta_{ri}) \times \hat{l}(\theta_{ri})$, that is tangent to the contact arc and changes orientation with θ_{ri}. This unit vector points into the page in the cross-section within

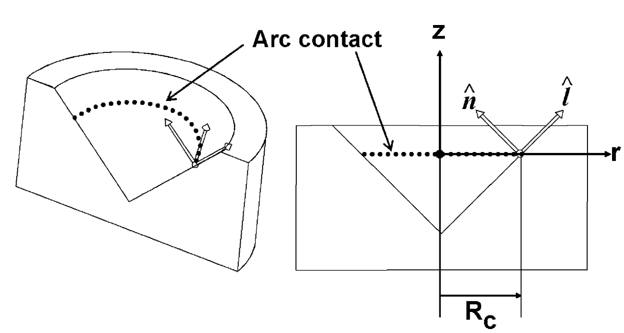

Fig. 17. Contact arc and $\hat{n}(\theta_{ri})$, $\hat{l}(\theta_{ri})$ coordinates for a cross-section at $\theta = \theta_{ri}$.

Fig. 17. In Eq. (A.5) we calculate the resultant force on the arc contact via a line integral along the arc of contact.

$$\vec{F}_j = \int_{s_{\text{initial}}}^{s_{\text{final}}} [f_n(\theta_{ri})\hat{n}(\theta_{ri}) + f_l(\theta_{ri})\hat{l}(\theta_{ri}) + f_s(\theta_{ri})\hat{s}(\theta_{ri})]\,\mathrm{d}s \approx \int_{\theta_{jr\,\text{initial}}}^{\theta_{jr\,\text{final}}} [f_n(\theta_r)\hat{n}(\theta_{ri})]R_c\,\mathrm{d}\theta_{ri} \quad (\text{A.5})$$

The limits of the integral are defined by the ends of the arc contact as illustrated in Fig. 5B. The subscripts n, l, and s differentiate between unit contact forces in the subscripted directions. It is good design practice to minimize friction ($\mu_{\text{static}} < 0.10$) at a coupling's contacts to prevent tangential stress build up. In Eq. (A.5) we have assumed this practice in QKC design and take the contribution of the tangential contact forces (in the l and s directions) as negligible compared to the contribution of the normal forces. If a rare application requires the tangential components, they can be added to the analysis. Using Eqs. (A.4) and (A.5) simplifies to Eq. (A.6).

$$\vec{F}_j = \int_{\theta_{jr\,\text{initial}}}^{\theta_{jr\,\text{final}}} \{K[\delta_n(\theta_{ri})]^b \hat{n}(\theta_{ri})\} R_c\,\mathrm{d}\theta_{ri} \quad (\text{A.6})$$

We now use the matrix in Eq. (A.7) to transform the unit contact force into the frame of the CCS.

$$\begin{bmatrix} \hat{n}(\theta_{ri}) \\ \hat{s}(\theta_{ri}) \\ \hat{l}(\theta_{ri}) \end{bmatrix} = \begin{bmatrix} -\cos(\theta_{ri})\cos(\theta_c) & -\sin(\theta_{ri})\cos(\theta_c) & \sin(\theta_c) \\ -\sin(\theta_{ri}) & \cos(\theta_{ri}) & 0 \\ \cos(\theta_{ri})\sin(\theta_c) & \sin(\theta_{ri})\sin(\theta_c) & \cos(\theta_c) \end{bmatrix} \times \begin{bmatrix} \hat{i} \\ \hat{j} \\ \hat{k} \end{bmatrix} \quad (\text{A.7})$$

In combining Eqs. (A.6) and (A.7) we obtain Eq. (A.8) which provides the total reaction force for contact arc j:

$$\vec{F}_j = \begin{bmatrix} \int_{\theta_{jr\,\text{initial}}}^{\theta_{jr\,\text{final}}} \{R_c\,K(\delta_n(\theta_{ri}))^b[-\cos(\theta_{ri})\cos(\theta_c)]\,\mathrm{d}\theta_{ri}\} & \hat{i} \\ \int_{\theta_{jr\,\text{initial}}}^{\theta_{jr\,\text{final}}} \{R_c\,K(\delta_n(\theta_{ri}))^b[-\sin(\theta_{ri})\cos(\theta_c)]\,\mathrm{d}\theta_{ri}\} & \hat{j} \\ \int_{\theta_{jr\,\text{initial}}}^{\theta_{jr\,\text{final}}} \{R_c\,K(\delta_n(\theta_{ri}))^b[\sin(\theta_c)]\,\mathrm{d}\theta_{ri}\} & \hat{k} \end{bmatrix} \quad (\text{A.8})$$

When the contact forces are summed over six contact arcs as in Eq. (A.9), we obtain the reaction force between the mated components.

$$\vec{F}_{\text{Reaction}} = \sum_{j=1}^{6} \vec{F}_j \quad (\text{A.9})$$

The reaction torque in Eq. (A.10) is the sum of torques about the coupling centroid due to each ball–groove reaction force ($\vec{F}_i$) and moment arm ($\vec{r}_{SI_i}$) between the CCS and the respective ball's SI$_i$.

$$\vec{T}_{\text{Reaction}} = \sum_{i=1}^{3} \vec{r}_{SI_i} \times \vec{F}_i \quad (\text{A.10})$$

A.6. Step 6: stiffness calculation

After specifying a preload displacement, the coupling stiffness in the direction of the error displacement is calculated by dividing the change in reaction forces by the magnitude of the error displacement:

$$k_{\text{imposed}} = \frac{\mathrm{d}(\text{Reaction})}{\mathrm{d}(\text{Imposed error displacement})} \quad (\text{A.11})$$

When we apply linear displacements, the reaction is the force given by Eq. (A.9). When we apply rotation displacements, the reaction is the torque given by Eq. (A.10).

Appendix B. Theory implemented in MathCAD program

The MathCAD program discussed in Section 4 is appended for inspection. The tool is available for download at http://psdam.mit.edu.

QUASI KINEMATIC COUPLING STIFFNESS MODELING TOOL

CHANE ONLY VARIABLES IN SHADED BOXES, ALL OTHERS ARE CALCULATED VALUES:

LOCATION OF JOINTS IN X, Y. LOCATION OF COUPLING PLANE IN Z

Location of joint coordinate systems (JCSi) relative to an arbitrary coordinate system:
Worksheet will calculate the position of the coupling centroid based on this input.

JCS3 must be left most joint, JCS2 is right most joint, JCS1 has greater y value than JCS2 and JCS3

$$JCS_i := \begin{pmatrix} x \cdot in \\ y \cdot in \\ z \cdot in \end{pmatrix} \qquad JCS_1 := \begin{pmatrix} 0.0000 \cdot in \\ 3.0000 \cdot in \\ 0 \cdot in \end{pmatrix}$$

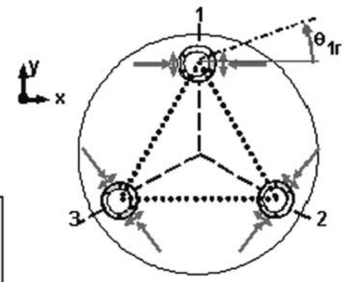

$$JCS_3 := \begin{pmatrix} -2.5981 \cdot in \\ -1.5000 \cdot in \\ JCS1_2 \end{pmatrix} \qquad JCS_2 := \begin{pmatrix} 2.5981 \cdot in \\ -1.5000 \cdot in \\ JCS1_2 \end{pmatrix}$$

Definition of joint positions

Calculate position of coupling centroid (xcc, ycc, zcc) relative to arbitrary coordinate system:

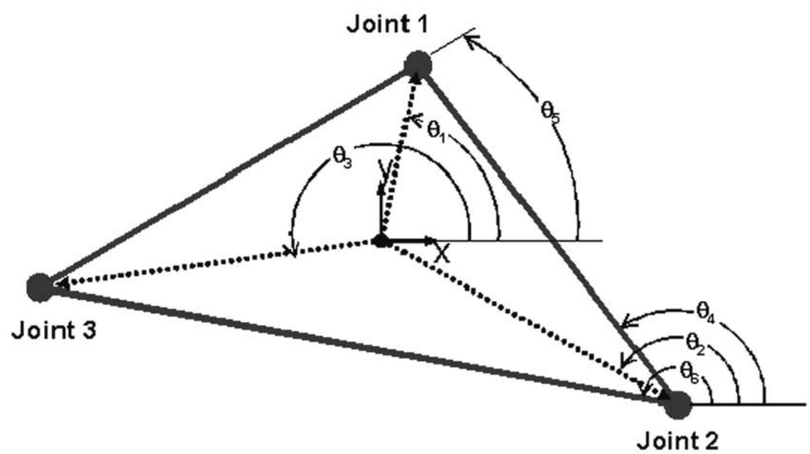

Definition of coupling triangle's bisector angles and side angles

$\theta_4 := \mathrm{atan2}\left(JCS1_0 - JCS2_0, JCS1_1 - JCS2_1\right)$ $\qquad$ $\theta_5 := \mathrm{atan2}\left(JCS1_0 - JCS3_0, JCS1_1 - JCS3_1\right)$

$\theta_6 := \mathrm{atan2}\left(JCS3_0 - JCS2_0, JCS3_1 - JCS2_1\right)$

$\theta_1 := \frac{1}{2} \cdot \left(\theta_4 + \theta_5\right)$ $\qquad$ $\theta_2 := \frac{1}{2} \cdot \left(\theta_4 + \theta_6\right)$ $\qquad$ $\theta_3 := \frac{1}{2} \cdot \left[\left(\theta_5 + \theta_6\right) + \pi\right]$

$$CCS_x := \frac{\left(JCS3_1 - JCS2_1 - \tan\left(\theta_3\right) \cdot JCS3_0 + \tan\left(\theta_2\right) \cdot JCS2_0\right)}{\tan\left(\theta_2\right) - \tan\left(\theta_3\right)}$$

$CCS_y := \tan\left(\theta_2\right) \cdot \left(CCS_x - JCS2_0\right) + JCS2_1$ $\qquad$ $CCS_z := JCS1_2$

Coupling Coordinate System Relative To Arbitrary Coordinate System:

$$CCS_{cc} := \begin{pmatrix} CCS_x \\ CCS_y \\ CCS_z \end{pmatrix} \qquad CCS_{cc} = \begin{pmatrix} 0.0000 \\ 0.0000 \\ 0.0000 \end{pmatrix} \mathrm{in}$$

Joint Coordinate System Positions Vectors Relative To Coupling Center:

$r_{JCS1} := JCS_1 - CCS_{cc}$ $\qquad$ $r_{JCS2} := JCS_2 - CCS_{cc}$ $\qquad$ $r_{JCS3} := JCS_3 - CCS_{cc}$

$\left|r_{JCS1}\right| = 3\,\mathrm{in}$ $\qquad$ $\left|r_{JCS2}\right| = 3\,\mathrm{in}$ $\qquad$ $\left|r_{JCS3}\right| = 3\,\mathrm{in}$

JOINT DIMENSIONS AND CONTACT CHARACTERISTICS

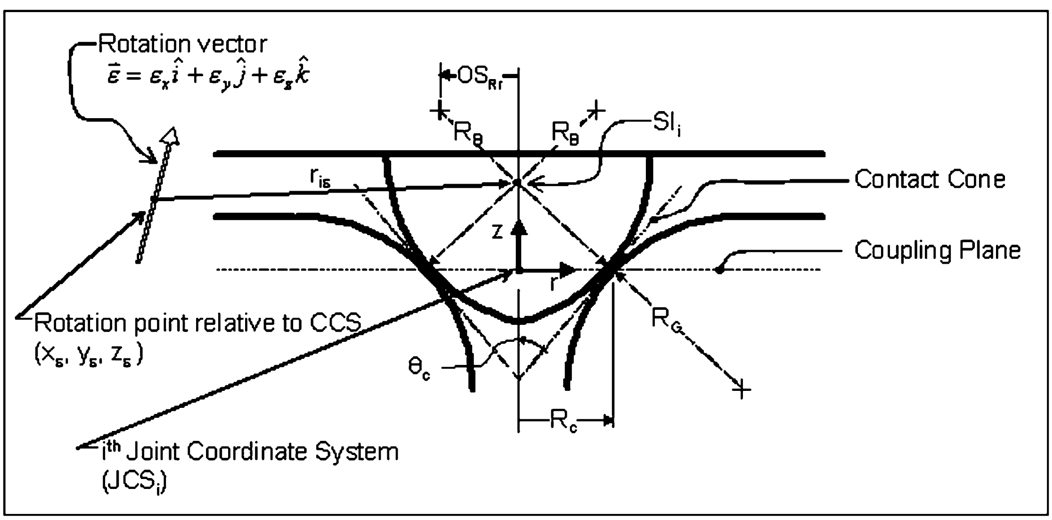

Half Cone Angle: $\theta_c := 45 \cdot \mathrm{deg}$

Ball Center Radial Offset: (shown negative in A-3) $O_{SRr} := -0.0752 \cdot \mathrm{in}$

Ball Radius: $R_B := 0.3946 \cdot \mathrm{in}$

Contact Radius: $R_c := R_B \cdot \cos(\theta_c) + O_{SRr}$

Tangential Stiffness/Resistance Coefficients:
set = 0 per assumptions in section 3.6

$\mu_{T1} := 0$ $\mu_{Ts} := 0$

Groove Contact Angle

$\theta_{contact} \equiv 120 \cdot \mathrm{deg}$

Pre-load Vector
relative to Coupling Coordinate System (CCS):

$$\delta_{preload} := \begin{pmatrix} 0 \dfrac{0.0002}{5.08} \cdot \mathrm{in} \\ 0 \dfrac{0.0002}{5.08} \cdot \mathrm{in} \\ -10 \dfrac{0.0002}{5.08} \cdot \mathrm{in} \end{pmatrix}$$

Error Translation Vector
relative to Coupling Coordinate System (CCS):

$$\delta_{error} := \begin{pmatrix} 0 \dfrac{0.0002}{5.08} \cdot \mathrm{in} \\ 0 \dfrac{0.0002}{5.08} \cdot \mathrm{in} \\ 0 \dfrac{0.0002}{5.08} \cdot \mathrm{in} \end{pmatrix}$$

Rotation Vector and Point of Rotation
relative to Coupling Coordinate System (CCS)

$$\varepsilon := \begin{bmatrix} (0 \cdot 10^{-6}) \\ (0 \cdot 10^{-6}) \\ (0 \cdot 10^{-6}) \end{bmatrix} \cdot \mathrm{rad} \qquad r_\varepsilon := \begin{pmatrix} 0 \\ 0 \\ 0 \end{pmatrix} \cdot \mathrm{in}$$

$$\delta_c := \delta_{preload} + \delta_{error}$$

VARIABLES FOR CONTACT MECHANICS AND UNIT CONTACT FORCES

VARIABLES FOR NORMAL CONTACT FORCE VS. DISPLACEMENT CURVE FIT:

Joint 1

$b_1 := 1.07$

$c_1 := 1 + b_1$

$K_1 := 2948850 \dfrac{\mathrm{lbf}}{\mathrm{in}^{c_1}}$

Joint 2

$b_2 := 1.07$

$c_2 := 1 + b_2$

$K_2 := 2948850 \dfrac{\mathrm{lbf}}{\mathrm{in}^{c_1}}$

Joint 3

$b_3 := 1.07$

$c_3 := 1 + b_3$

$K_3 := 2948850 \dfrac{\mathrm{lbf}}{\mathrm{in}^{c_1}}$

---------------------------------- END USER INPUT ----------------------------------
PROCEED TO END OF SHEET FOR CALCULATED REACTION FORCE/TORQUE

ANGLE LIMITS OF ARC CONTACTS

Arc Contact Angular Limits (used for line contact integration):

$\theta_{jrfinal}$ must ALWAYS be greater than in $\theta_{jrinitial}$ and numeric values of both must be less than or equal to 360 degrees. For example, consider when a contact crosses the x axis (See A-4)

- Incorrect assignment: $\theta_{jrfinal} = 60°$ and $\theta_{jrinitial} = 300°$
- Correct assignment: $\theta_{jrfinal} = 60°$ and $\theta_{jrinitial} = -60°$

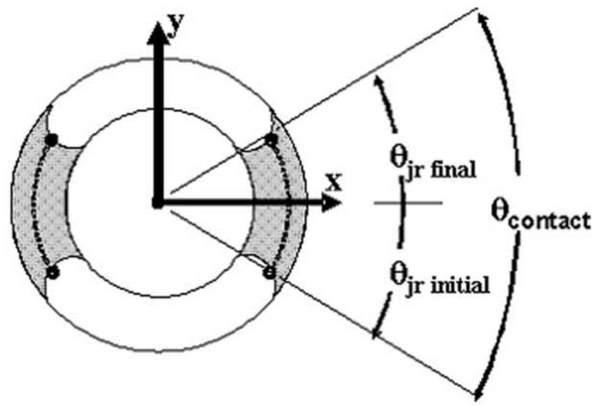

Fig. A-4: Definition of contact angles [i.e. for $\theta_{rf} = 60°$ and $\theta_{ri} = -60°$]

Joint 1, FIRST ARC, j = 1:

$\theta_{1rinitial} := \theta_1 + \frac{(\pi - \theta_{contact})}{2}$ $\quad \theta_{1rfinal} := \theta_{1rinitial} + \theta_{contact}$ $\quad \theta_{1rinitial} = 120\ deg$ $\quad \theta_{1rfinal} = 240\ deg$

Joint 1, SECOND ARC, j = 2:

$\theta_{2rinitial} := \theta_{1rinitial} - \pi$ $\quad \theta_{2rfinal} := \theta_{2rinitial} + \theta_{contact}$ $\quad \theta_{2rinitial} = -60\ deg$ $\quad \theta_{2rfinal} = 60\ deg$

Joint 2, FIRST ARC, j = 3:

$\theta_{3rinitial} := \theta_2 + \frac{(-\pi - \theta_{contact})}{2}$ $\quad \theta_{3rfinal} := \theta_{3rinitial} + \theta_{contact}$ $\quad \theta_{3rinitial} = 0\ deg$ $\quad \theta_{3rfinal} = 120\ deg$

Joint 2, SECOND ARC, j = 4:

$\theta_{4rinitial} := \theta_{3rinitial} + \pi$ $\quad \theta_{4rfinal} := \theta_{4rinitial} + \theta_{contact}$ $\quad \theta_{4rinitial} = 180\ deg$ $\quad \theta_{4rfinal} = 300\ deg$

Joint 3, FIRST ARC, j = 5:

$\theta_{5rinitial} := \theta_3 + \frac{(\pi - \theta_{contact})}{2}$ $\quad \theta_{5rfinal} := \theta_{5rinitial} + \theta_{contact}$ $\quad \theta_{5rinitial} = 240\ deg$ $\quad \theta_{5rfinal} = 360\ deg$

Joint 3, SECOND ARC, j = 6:

$\theta_{6rinitial} := \theta_{5rinitial} - \pi$ $\quad \theta_{6rfinal} := \theta_{6rinitial} + \theta_{contact}$ $\quad \theta_{6rinitial} = 60\ deg$ $\quad \theta_{6rfinal} = 180\ deg$

CALCULATED POSITION CHANGE OF SYMMETRY INTERCEPTS

$$r_{SI1} := r_{JCS1} + \begin{pmatrix} 0 \\ 0 \\ R_c \cdot \tan(\theta_c) \end{pmatrix} \qquad r_{SI2} := r_{JCS2} + \begin{pmatrix} 0 \\ 0 \\ R_c \cdot \tan(\theta_c) \end{pmatrix} \qquad r_{SI3} := r_{JCS3} + \begin{pmatrix} 0 \\ 0 \\ R_c \cdot \tan(\theta_c) \end{pmatrix}$$

$$r_{1\varepsilon} := r_{SI1} - r_\varepsilon \qquad r_{2\varepsilon} := r_{SI2} - r_\varepsilon \qquad r_{3\varepsilon} := r_{SI3} - r_\varepsilon$$

$$\delta_{SI1} := \delta_c + \varepsilon \times r_{1\varepsilon} \qquad \delta_{SI2} := \delta_c + \varepsilon \times r_{2\varepsilon} \qquad \delta_{SI3} := \delta_c + \varepsilon \times r_{3\varepsilon}$$

$$\delta_{SI1} = \begin{pmatrix} 0.00000 \\ 0.00000 \\ -0.00039 \end{pmatrix} \text{in} \qquad \delta_{SI2} = \begin{pmatrix} 0.00000 \\ 0.00000 \\ -0.00039 \end{pmatrix} \text{in} \qquad \delta_{SI3} = \begin{pmatrix} 0.00000 \\ 0.00000 \\ -0.00039 \end{pmatrix} \text{in}$$

IN-PLANE TRANSLATION OF SYMMETRY INTERCEPTS

$$\delta_{1rmax} := \left[\left(\delta_{SI1_0}\right)^2 + \left(\delta_{SI1_1}\right)^2\right]^{\frac{1}{2}} \qquad \delta_{2rmax} := \left[\left(\delta_{SI2_0}\right)^2 + \left(\delta_{SI2_1}\right)^2\right]^{\frac{1}{2}} \qquad \delta_{3rmax} := \left[\left(\delta_{SI3_0}\right)^2 + \left(\delta_{SI3_1}\right)^2\right]^{\frac{1}{2}}$$

$$\delta_{1rmax} = 0\,\text{in} \qquad \delta_{2rmax} = 0\,\text{in} \qquad \delta_{3rmax} = 0\,\text{in}$$

$$\theta_{1rmax} := \text{atan2}\left(\delta_{SI1_0}, \delta_{SI1_1} + 10^{-99} \cdot \text{in}\right) \qquad \theta_{2rmax} := \text{atan2}\left(\delta_{SI2_0}, \delta_{SI2_1} + 10^{-99} \cdot \text{in}\right)$$

$$\theta_{3rmax} := \text{atan2}\left(\delta_{SI3_0}, \delta_{SI3_1} + 10^{-99} \cdot \text{in}\right)$$

$$\theta_{1rmax} = 90\,\text{deg} \qquad \theta_{2rmax} = 90\,\text{deg} \qquad \theta_{3rmax} = 90\,\text{deg}$$

NORMAL DISPLACEMENT FUNCTIONS

$$\delta_{1n}(\theta_r) := -\delta_{1rmax} \cdot \cos(\theta_r - \theta_{1rmax}) \cdot \cos(\theta_c) + \delta_{SI1_2} \cdot \sin(\theta_c)$$

$$\delta_{2n}(\theta_r) := -\delta_{2rmax} \cdot \cos(\theta_r - \theta_{2rmax}) \cdot \cos(\theta_c) + \delta_{SI2_2} \cdot \sin(\theta_c)$$

$$\delta_{3n}(\theta_r) := -\delta_{3rmax} \cdot \cos(\theta_r - \theta_{3rmax}) \cdot \cos(\theta_c) + \delta_{SI3_2} \cdot \sin(\theta_c)$$

FUNCTIONS FOR UNIT FORCE VS DISTANCE OF APPROACH

$$f_{n1}(\theta_r) := K_1 \cdot \left(\left|\delta_{1n}(\theta_r)\right|\right)^{b_1} \qquad f_{n2}(\theta_r) := K_2 \cdot \left(\left|\delta_{2n}(\theta_r)\right|\right)^{b_2} \qquad f_{n3}(\theta_r) := K_3 \cdot \left(\left|\delta_{3n}(\theta_r)\right|\right)^{b_3}$$

BALL-GROOVE CONTACT ARC FORCES

Provides the force on groove surfaces, NOT the force on the ball surface(s)

JOINT 1, FIRST ARC, j = 1:

$$F_{j1} := R_c \cdot \begin{bmatrix} \displaystyle\int_{\theta_{1rinitial}}^{\theta_{1rfinal}} -f_{n1}(\theta_r) \cdot \left(-\cos(\theta_r) \cdot \cos(\theta_c) - \mu_{Ts} \cdot \sin(\theta_r) + \mu_{Tl} \cdot \cos(\theta_r) \cdot \sin(\theta_c)\right) d\theta_r \\ \displaystyle\int_{\theta_{1rinitial}}^{\theta_{1rfinal}} -f_{n1}(\theta_r) \cdot \left(-\sin(\theta_r) \cdot \cos(\theta_c) + \mu_{Ts} \cdot \cos(\theta_r) + \mu_{Tl} \cdot \sin(\theta_r) \cdot \sin(\theta_c)\right) d\theta_r \\ \displaystyle\int_{\theta_{1rinitial}}^{\theta_{1rfinal}} -f_{n1}(\theta_r) \cdot \left(\sin(\theta_c) + \mu_{Tl} \cdot \cos(\theta_c)\right) d\theta_r \end{bmatrix}$$

JOINT 1, SECOND ARC, j = 2:

$$F_{j2} := R_c \cdot \begin{bmatrix} \displaystyle\int_{\theta_{2rinitial}}^{\theta_{2rfinal}} -f_{n1}(\theta_r) \cdot \left(-\cos(\theta_r) \cdot \cos(\theta_c) - \mu_{Ts} \cdot \sin(\theta_r) + \mu_{Tl} \cdot \cos(\theta_r) \cdot \sin(\theta_c)\right) d\theta_r \\ \displaystyle\int_{\theta_{2rinitial}}^{\theta_{2rfinal}} -f_{n1}(\theta_r) \cdot \left(-\sin(\theta_r) \cdot \cos(\theta_c) + \mu_{Ts} \cdot \cos(\theta_r) + \mu_{Tl} \cdot \sin(\theta_r) \cdot \sin(\theta_c)\right) d\theta_r \\ \displaystyle\int_{\theta_{2rinitial}}^{\theta_{2rfinal}} -f_{n1}(\theta_r) \cdot \left(\sin(\theta_c) + \mu_{Tl} \cdot \cos(\theta_c)\right) d\theta_r \end{bmatrix}$$

$$F_{i1} := F_{j1} + F_{j2}$$

JOINT 2, FIRST ARC, j = 3:

$$F_{j3} := R_c \cdot \begin{bmatrix} \displaystyle\int_{\theta_{3rinitial}}^{\theta_{3rfinal}} -f_{n2}(\theta_r) \cdot \left(-\cos(\theta_r) \cdot \cos(\theta_c) - \mu_{Ts} \cdot \sin(\theta_r) + \mu_{Tl} \cdot \cos(\theta_r) \cdot \sin(\theta_c)\right) d\theta_r \\ \displaystyle\int_{\theta_{3rinitial}}^{\theta_{3rfinal}} -f_{n2}(\theta_r) \cdot \left(-\sin(\theta_r) \cdot \cos(\theta_c) + \mu_{Ts} \cdot \cos(\theta_r) + \mu_{Tl} \cdot \sin(\theta_r) \cdot \sin(\theta_c)\right) d\theta_r \\ \displaystyle\int_{\theta_{3rinitial}}^{\theta_{3rfinal}} -f_{n2}(\theta_r) \cdot \left(\sin(\theta_c) + \mu_{Tl} \cdot \cos(\theta_c)\right) d\theta_r \end{bmatrix}$$

JOINT 2, SECOND ARC, j = 4:

$$F_{j4} := R_c \cdot \begin{bmatrix} \int_{\theta_{4rinitial}}^{\theta_{4rfinal}} -f_{n2}(\theta_r) \cdot \left(-\cos(\theta_r) \cdot \cos(\theta_c) - \mu_{Ts} \cdot \sin(\theta_r) + \mu_{Tl} \cdot \cos(\theta_r) \cdot \sin(\theta_c)\right) d\theta_r \\ \int_{\theta_{4rinitial}}^{\theta_{4rfinal}} -f_{n2}(\theta_r) \cdot \left(-\sin(\theta_r) \cdot \cos(\theta_c) + \mu_{Ts} \cdot \cos(\theta_r) + \mu_{Tl} \cdot \sin(\theta_r) \cdot \sin(\theta_c)\right) d\theta_r \\ \int_{\theta_{4rinitial}}^{\theta_{4rfinal}} -f_{n2}(\theta_r) \cdot \left(\sin(\theta_c) + \mu_{Tl} \cdot \cos(\theta_c)\right) d\theta_r \end{bmatrix}$$

$$F_{i2} := F_{j3} + F_{j4}$$

JOINT 3, FIRST ARC, j = 5:

$$F_{j5} := R_c \cdot \begin{bmatrix} \int_{\theta_{5rinitial}}^{\theta_{5rfinal}} -f_{n3}(\theta_r) \cdot \left(-\cos(\theta_r) \cdot \cos(\theta_c) - \mu_{Ts} \cdot \sin(\theta_r) + \mu_{Tl} \cdot \cos(\theta_r) \cdot \sin(\theta_c)\right) d\theta_r \\ \int_{\theta_{5rinitial}}^{\theta_{5rfinal}} -f_{n3}(\theta_r) \cdot \left(-\sin(\theta_r) \cdot \cos(\theta_c) + \mu_{Ts} \cdot \cos(\theta_r) + \mu_{Tl} \cdot \sin(\theta_r) \cdot \sin(\theta_c)\right) d\theta_r \\ \int_{\theta_{5rinitial}}^{\theta_{5rfinal}} -f_{n3}(\theta_r) \cdot \left(\sin(\theta_c) + \mu_{Tl} \cdot \cos(\theta_c)\right) d\theta_r \end{bmatrix}$$

JOINT 3, FIRST ARC, j = 6:

$$F_{j6} := R_c \cdot \begin{bmatrix} \int_{\theta_{6rinitial}}^{\theta_{6rfinal}} -f_{n3}(\theta_r) \cdot \left(-\cos(\theta_r) \cdot \cos(\theta_c) - \mu_{Ts} \cdot \sin(\theta_r) + \mu_{Tl} \cdot \cos(\theta_r) \cdot \sin(\theta_c)\right) d\theta_r \\ \int_{\theta_{6rinitial}}^{\theta_{6rfinal}} -f_{n3}(\theta_r) \cdot \left(-\sin(\theta_r) \cdot \cos(\theta_c) + \mu_{Ts} \cdot \cos(\theta_r) + \mu_{Tl} \cdot \sin(\theta_r) \cdot \sin(\theta_c)\right) d\theta_r \\ \int_{\theta_{6rinitial}}^{\theta_{6rfinal}} -f_{n3}(\theta_r) \cdot \left(\sin(\theta_c) + \mu_{Tl} \cdot \cos(\theta_c)\right) d\theta_r \end{bmatrix}$$

$$F_{i3} := F_{j5} + F_{j6}$$

FORCE ON EACH ARC CONTACT AND BETWEEN BALL AND GROOVE

$$F_{j1} = \begin{pmatrix} -116 \\ 0 \\ -140 \end{pmatrix} \text{lbf} \qquad F_{j2} = \begin{pmatrix} 116 \\ 0 \\ -140 \end{pmatrix} \text{lbf} \qquad F_{i1} = \begin{pmatrix} 0 \\ 0 \\ -279 \end{pmatrix} \text{lbf}$$

$$F_{j3} = \begin{pmatrix} 58 \\ 100 \\ -140 \end{pmatrix} \text{lbf} \qquad F_{j4} = \begin{pmatrix} -58 \\ -100 \\ -140 \end{pmatrix} \text{lbf} \qquad F_{i2} = \begin{pmatrix} -0 \\ 0 \\ -279 \end{pmatrix} \text{lbf}$$

$$F_{j5} = \begin{pmatrix} 58 \\ -100 \\ -140 \end{pmatrix} \text{lbf} \qquad F_{j6} = \begin{pmatrix} -58 \\ 100 \\ -140 \end{pmatrix} \text{lbf} \qquad F_{i3} = \begin{pmatrix} 0 \\ 0 \\ -279 \end{pmatrix} \text{lbf}$$

REACTION FORCE AND TORQUE

$$F_{Reaction} := F_{j1} + F_{j2} + F_{j3} + F_{j4} + F_{j5} + F_{j6}$$

$$\boxed{F_{Reaction} = \begin{pmatrix} 0 \\ 0 \\ -838 \end{pmatrix} \text{lbf}}$$

$$F_{radial} := \left[\left(F_{Reaction_0}\right)^2 + \left(F_{Reaction_1}\right)^2\right]^{\frac{1}{2}}$$

$$\boxed{F_{radial} = 0\,\text{lbf}}$$

$$T_{Reaction} := r_{SI1} \times F_{i1} + r_{SI2} \times F_{i2} + r_{SI3} \times F_{i3}$$

$$\boxed{T_{Reaction} = \begin{pmatrix} 0 \\ 0 \\ 0 \end{pmatrix} \text{in} \cdot \text{lbf}}$$

VERIFY CONSTANT CONTACT CONDITION

Should the any of these graphs cross $\delta_{ni}(\theta_r) = 0$; the analysis is not valid

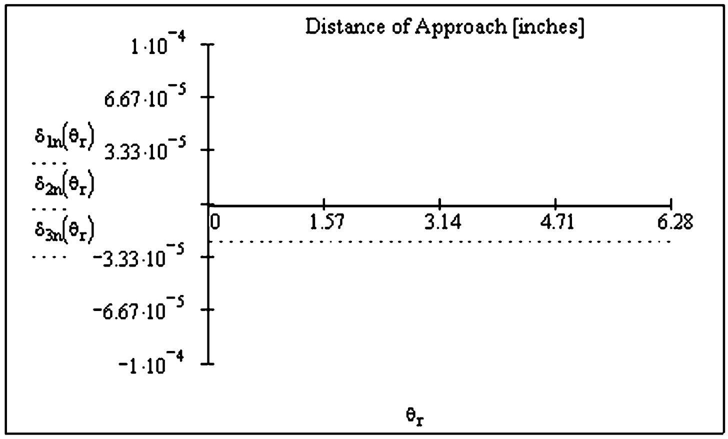

Fig. A-5: Constant Contact Assumption Monitor Plot

STIFFNESS CALCULATION

PROCEDURE (LINEARIZE FOR SMALL DISPLACEMENTS):

- IMPOSE PRELOAD ON THE JOINT, RECORD CORRESPONDING REACTION (R_1)
- IMPOSE AN ERROR Δ_s (LINEAR OR ROTARY) &RECORD CORRESPONDING REACTION (R_2)

$k \sim$ absolute $| (R_2 - R_1) / \Delta_s |$

References

[1] Slocum AH. Kinematic couplings for precision fixturing—Part I. Formulation of design parameters. Prec Eng 1988;10:85–91.
[2] Slocum AH. Design of three-groove kinematic couplings. Prec Eng 1992;14:67–73.
[3] Slocum AH, Mueller L, Braunstein D. Flexural mount kinematic couplings and method. United States Patent 5,678,944.
[4] Culpepper ML, Slocum AH, Shaikh FZ. Compliant kinematic couplings for use in manufacturing and assembly. In: Proceedings of the 1998 ASME International Mechanical Engineering Congress and Exposition, Anaheim, CA; 1998. p. 611–8.
[5] Suh NP. In pursuit of the lower limit of friction coefficient in dry sliding. In: Proceedings of the 1993 ASME Winter Annual Meeting, New Orleans, LA; 1993. p. 1–8.
[6] Johnson KL. Deformation of a plastic wedge by a rigid flat die under the action of a tangential force. J Mechan Phys Solids 1968;16:395–402.
[7] Childs THC. The persistence of asperities in indentation experiments. Wear 1973;25:3–17.
[8] Schmiechen P, Slocum AH. Analysis of kinematic systems: a generalized approach. Prec Eng 1996;19:11–8.
[9] Hale LC, Slocum AH. Optimal design techniques for kinematic couplings. Prec Eng 2001;25:114–27.
[10] Schouten CH, Rosielle PCJN, Schellekens PHJ. Design of a kinematic coupling for precision applications. Prec Eng 1997;20:46–52.
[11] Culpepper ML, Slocum AH, Shaikh FZ. Quasi-kinematic couplings for precision automotive assemblies. In: Proceedings of the 1999 ASME-ICE Fall Conference, Ann Arbor, MI; 1999. p. 61–6.
[12] Culpepper ML. Design and application of compliant quasi-kinematic couplings. Ph.D. Thesis, MIT, Cambridge, MA; 2000. p. 89–108.
[13] Culpepper ML, Slocum AH, Shaikh FZ, Vrsek G. Quasi-kinematic couplings for low-cost precision alignment of high-volume assemblies. ASME J Mechan Des 2004;126(in press).
[14] Hale LC. Principles and techniques for designing precision machines. Ph.D. Thesis, MIT, Cambridge, MA; 1999.
[15] Slocum AH, Donmez A. Kinematic couplings for precision fixturing—Part 2. Experimental determination of repeatability and stiffness. Prec Eng 1988;10:115–22.
[16] Johnson KL. Contact mechanics. Cambridge, UK: Cambridge University Press; 1985. p. 85–9.
[17] Oiwa T, Kyusojin A. Development of precise cylindrical grinding by ball centers-contact stiffness between ball and centre hole. Prec Eng 1999;12:37–42.